NRL Report 8320
EOTPO Report No. 52

Passive Infrared Surveillance, Part I: Model Formulation

RICHARD A. STEINBERG

Electro-Optical Technology Program Office (EOTPO)
Management Information and Special Programs Organization

September 28, 1979

ELECTRO-OPTICAL TECHNOLOGY PROGRAM OFFICE
NAVAL RESEARCH LABORATORY
Washington, D.C. 20375

Reviewed and approved by:

Dr. John M. MacCallum, Jr.
Head, Electro-Optical Technology Program Office

SECURITY CLASSIFICATION OF THIS PAGE (When Data Entered)

REPORT DOCUMENTATION PAGE

READ INSTRUCTIONS BEFORE COMPLETING FORM

1 REPORT NUMBER: NRL Report 8320	2 GOVT ACCESSION NO
3 RECIPIENT'S CATALOG NUMBER	
4 TITLE (and Subtitle): PASSIVE INFRARED SURVEILLANCE PART I: MODEL FORMULATION	5 TYPE OF REPORT & PERIOD COVERED: Interim report on a continuing NRL Problem.
6 PERFORMING ORG. REPORT NUMBER: EOTPO Report 5	
7 AUTHOR(s): Richard A. Steinberg	8 CONTRACT OR GRANT NUMBER(s)
9 PERFORMING ORGANIZATION NAME AND ADDRESS: Naval Research Laboratory, Washington, D.C. 20375	10 PROGRAM ELEMENT, PROJECT, TASK AREA & WORK UNIT NUMBERS: NRL Problem N01-29
11 CONTROLLING OFFICE NAME AND ADDRESS: Chief of Naval Material, Washington, D.C. 20360	12 REPORT DATE: September 28, 1979 13 NUMBER OF PAGES: 41
14 MONITORING AGENCY NAME & ADDRESS (if different from Controlling Office)	15 SECURITY CLASS. (of this report): Unclassified 15a DECLASSIFICATION DOWNGRADING SCHEDULE

16 DISTRIBUTION STATEMENT (of this Report)

Approved for public release, distribution unlimited.

17 DISTRIBUTION STATEMENT (of the abstract entered in Block 20, if different from Report)

18 SUPPLEMENTARY NOTES

19 KEY WORDS (Continue on reverse side if necessary and identify by block number)

Infrared technology
Electro-Optical Technology Program Office (EOTPO)
Electro-Optics
Surveillance

20 ABSTRACT (Continue on reverse side if necessary and identify by block number)

A new theoretical procedure is presented for calculating the performance of scanning background-limited (BLIP) infrared sensors with adaptive threshold signal-processing logic. The performance predictions obtained with this model are background-conditional, i.e., are valid only for a given infrared background scene, presumably specified as a radiance map of arbitrary (but deterministic) structure. The nonstationary statistical nature of the photocurrent is explicitly taken into account. The basic approach involves a combination of some results from optical communications theory with a

(continued)

DD FORM 1 JAN 73 1473 EDITION OF 1 NOV 65 IS OBSOLETE

S/N 0102-014-6601

SECURITY CLASSIFICATION OF THIS PAGE (When Data Entered)

20. ABSTRACT (continued)

formalism for the threshold-crossing statistics of nonstationary noises, originally developed by Rice, Cramér, and Leadbetter. The present work is pursued further in a companion paper in which various simplifying approximations and illustrative numerical examples are presented. The theory developed in these two papers is directly applicable to design parameter trade-off studies for infrared search and track (IRST) devices.

CONTENTS

GLOSSARY OF SYMBOLS

Symbol	Initial Definition	
AT	p.22	Adaptive threshold
$\mathcal{A}_{det}$	Eq.(A-6)	Detector active area
BSL	p.23	Background structure limited (signal processor performance regime)
BLIP	p.5	Background (quantum noise) limited photodetector
CFAR	p.11	Constant false alarm rate
C	Eq.(29)	Covariance matrix (a submatrix of Λ)
C_{AB}	Eq.32	Scalar covariance (A and B may equal $Y, \dot{Y}, \dot{Y}_o$, etc.)
D_{ap}	Eq.(A-8)	Optical aperture diameter
e	Eq.(3)	Electronic charge
$E\{\cdot\}$	Eq.(1)	Statistical expectation operator (ensemble average)
$E_{Y_o \dot{Y}_o}\{\cdot\}$	Eq. (49)	Expectation on processes Y_o and $\dot{Y}_o$
E_J	Eq.(C-12)	Error term in the crossing count variance expression
f	p.7	Electrical frequency (Hz)
$\mathbf{f}$	Eq.(A-2)	Two-dimensional vector spatial frequency
$f^{\#}$	Eq.(A-3)	Optical focal length ratio
f_Y	Eq.(51)	Probability density function of the process $Y(t)$
$f_J(J)$	Eq.(C-2)	Probability density function of the crossing count J
$f_{Y\dot{Y}}$	Eq.(20)	Joint density function of Y and $\dot{Y}$
$f_{Y_o \dot{Y}_o}$	Eq.(20)	Joint density function of Y_o and $\dot{Y}_o$
$f_{Y\dot{Y}Y_o\dot{Y}_o}$	Eq.(20)	Joint density function of Y, $\dot{Y}$, Y_o, and $\dot{Y}_o$
$F(\cdot)$	Eq.(67)	Crossing rate factor
FT	p.23	Fixed threshold
FAR	p.1	False alarm rate
FAR_{AT}	Eq.(86)	False alarm rate of adaptive threshold processor
FAR_{FT}	Eq.(86)	False alarm rate of fixed threshold processor
FAP	Eq.(87)	False alarm penalty
FLIR	p.1	Forward looking infrared (imaging system)
Δf	Eq.(7)	Noise equivalent bandwidth of $H(f)$
Δf_o	Eq.(72)	Noise equivalent bandwidth of $H_o(f)$
$h(t)$	p.9	Fourier inverse of $H(f)$; impulse response of the target channel
$H(f)$	p.4	Target channel transfer function
$H_o(f)$	p.4	Threshold channel transfer function
$h_o(t)$	Eq.(38)	Fourier inverse of $H_o(f)$
h	Eq.(A-4)	Planck's constant
IRST	p.1	Infrared search and track
J	p.9	The number of threshold crossings during a time interval
K	p.4	Gain constant
K_o	Eq.(A-3)	Ratio of focal plane irradiance to scene radiance
m_A	Eq.(33)	Expected value of $A(t)$; $A(t)$ may be $Y, \dot{Y}, \dot{Y}_o$, etc.
m_X	Eq.(3)	Expected value of the unfiltered current $X(t)$
m_Y	Eq.(4)	Expected value of the filtered current $Y(t)$
$m_J(O,T)$	Eq.(8)	Mean crossing count on the interval $\lvert t \rvert < T/2$

$\dot{m}_J(t)$	Eq.(9)	Threshold crossing rate
$\dot{m}_{J_0}$	Eq.(9)	Positive slope zero-crossing rate
$\hat{m}_Y$	Eq.(14)	Estimated value of m_Y
$\dot{m}_J(t\|y_0,\dot{y}_0)$	Eq.(48)	Threshold-conditional crossing rate
$m_L(\mathbf{r})$	p.27	Scene spatial radiance distribution
$m_{\mathcal{L}}(\mathbf{f})$	Eq.(A-2)	Two-dimensional Fourier transform of $m_L(\mathbf{f})$
m_Q	Eq.(3)	Average photon flux incident on detector
MTF(f)	Eq.(A-2)	Modulation transfer function
N	p.25	Number of taps on the Fig. 10 delay line
$P(\mathbf{r})$	Eq.(A-6)	"Pupil function" of a focal plane detector
$\mathcal{P}(\mathbf{f})$	Eq.(A-2)	Two-dimensional Fourier transform of $P(\mathbf{r})$
P_D	p.1	Probability of detection
p	Eq.(56)	Argument of crossing rate function
QNL	p.23	Quantum-noise-limited (signal processor performance regime)
$\mathbf{r}$	p.27	Two-dimensional focal plane location vector
R_I	Eq.(A-4)	Current responsivity of photodetector
$r(t)$	Eq.(52)	Correlation co-efficient of $Y(t)$ and $\dot{Y}(t)$
t	p.3	Time
T	Eq.(8)	Time interval
T_0	Eq.(12)	The time interval $\|t\| < T/2$
T_d	p.4	Delay time (sensor dwell time)
t_{mc}	Eq.(76)	Mean-crossing time
t_{ca}	Eq.(78)	Time of closest approach
T_F	Eq.(A-8)	System frame time
T_{ref}	Eq.(C-1)	Reference time interval for FAR calculation
TDI	p.25	Time delay and integration
TIS	p.27	Thermal imaging system
u	Eq.(11)	Normalized threshold level
$\mathbf{v}$	Eq.(A-8)	Focal plane scan velocity
$X(t)$	p.3	Unfiltered photocurrent
$Y(t)$	p.3	Filtered photocurrent
$Y_0(t)$	p.3	Threshold current
$y(t;n)$	Eq.(1)	Sample function of the random process $Y(t)$
y_0	Eq.(11)	Fixed threshold level
$\dot{Y}(t)$	p.13	Time derivative of $Y(t)$
$\dot{Y}_0(t)$	p.13	Time derivative of $Y_0(t)$
Z	Eq.(B-7)	Shorthand notation for $\dot{Y}(t)$
α	Eq.(90)	Ratio of noise bandwidths
$\delta(\cdot)$	Eq.(B-18)	Dirac delta function
∂_t	Eq.(B-8)	Partial derivative operator on variable t
$\Delta\lambda_1$	p.27	Spectral band
ϵ	Eq.(51)	Relative error term in Gaussian approximation to $f_Y(y)$
η	Eq.(3)	Detector quantum efficiency
Λ	Eq.(28)	Covariance matrix
ν	Eq.(A-4)	Optical frequency (Hz)
σ_Y	Eq.(2)	Standard deviation of $Y(t)$
$\sigma_{\dot{Y}}$	Eq.(B-12)	Standard deviation of $\dot{Y}(t)$

$\hat{\sigma}_\gamma$	Eq.(14)	Estimated value of σ_γ
$\dot{\sigma}_\gamma$	Eq.(B-23)	Time derivative of σ_γ
$\sigma_{\gamma\gamma_o}$	Eq.(68)	Root-sum-square of σ_γ and σ_{γ_o}
$\sigma_{\dot{\gamma}\dot{\gamma}_o}$	Eq.(69)	Root-sum-square of $\sigma_{\dot{\gamma}}$ and $\sigma_{\dot{\gamma}_o}$
σ_J	p.32	Standard deviation of J
τ_o	Eq.(A-3)	Transmittance of the optical train
$\phi(\cdot)$	Eq.(57)	Normalized Gaussian density
$\Phi(\cdot)$	Eq.(58)	Normalized Gaussian distribution
$\circledcirc$	Eq.(37a)	Convolution operator

PASSIVE INFRARED SURVEILLANCE
PART I: MODEL FORMULATION

INTRODUCTION

This paper describes an analytical model for predicting the performance of a particular class of infrared sensors generically described as infrared search and track (IRST) devices. An IRST system generally consists of one or more photodetectors located in the focal plane of a scanning optical telescope, and a complement of signal processing electronics to process the detected photocurrents. The signal processor's task is to determine whether or not an object of a particular type (a "target") is anywhere in the sensor's field of view, while keeping the frequency of false target reports to an acceptably low level.

Thus, the Neyman-Pearson criteria conventionally applied to radar systems is appropriate also as an objective of IRST processor design: the target detection probability (P_D) should be maximized for a given maximum tolerable false alarm rate (FAR).

The IRST is a nonimaging device, as contrasted with forward looking infrared (FLIR) imaging systems [1,2]. The search and track device may be required to keep a full hemisphere (2π steradians) under constant observation, to have a resolution of one milliradian or less, and to operate without human assistance for long periods of time. The challenge this presents to the system designer is further magnified by the abundant opportunities for target/background confusion offered by such typical background scenes as cloudy skies and cities.

Previous attempts to model background effects on IRST system performance have focused on the Wiener spectrum approach [3-9], a frequency domain technique originally developed for calculating the noise variance in communication circuits. Unfortunately, unlike the noise processes typically assumed in statistical communication theory [10,11], the IRST photocurrent is a highly non-stationary random process. As the sensor scans across a structured background, the spatially non-uniform scene brightness is mapped into a photocurrent whose mean and variance are both functions of time. The inadequacy of the Wiener spectrum method under these conditions has been appreciated for many years [12,13].

The IRST model developed in this paper requires as input complete descriptions of the IRST sensor and the scene radiance distribution (possibly including a target). As output, the model generates the probability that the IRST device declares (rightly or wrongly) a target's presence in the scene. *A priori* knowledge as to whether a target was in fact present in the specified scene allows interpretation of the probability of target declaration either as a probability of target detection (P_D) or as a "false alarm."

Photon fluctuation noise is the only stochastic aspect of the model; the background must be specified as a radiance map of arbitrary, but deterministic, structure. Thus, the performance predictions made with this model are background-conditional.

Manuscript submitted February 13, 1979

Previous works describing analysis techniques for IRST systems (e.g., Refs. 14 and 15) are restricted in validity to uniform scenes. The contribution of this paper is an original method for calculating IRST performance (i.e., the parameters P_D and FAR) that is inherently applicable to non-uniform scenes. The method described here can be used to assess the relative merits of a variety of IRST system concepts, all operating against a particular infrared scene. Alternatively, an IRST sensor's background-conditional performance can be evaluated for each member of an ensemble of scenes, in order to establish ensemble average performance statistics for a realistic range of operational environments.

Before launching into the main body of analysis, a treatment of the elementary concepts involved is first presented in the next section. The latter part of the subsection (Current Statistics) presents a brief discussion of how values for the mean and variance of a photocurrent (i.e., the "current statistics") are obtained from knowledge of the brightness of a presumably uniform background scene.

The final part of the next subsection (Crossing Rates for Fixed Threshold Detection) presents Rice's well-known equation, which is Eq. (9) in this text, for the threshold crossing rate of a stationary Gaussian random process [16]. Evaluation of Eq. (9) requires knowledge of the mean value and variance of the Gaussian process. A description of IRST performance against uniform background scenes is obtained by inserting the current statistics from the Current Statistics Subsection into Rice's equation, Eq. (9).

Rice's equation, by itself, is devoid of physical content: it applies equally well to any stationary Gaussian process. All of the physical parameters—the optical and electrical characteristics of the IRST sensor and the radiance of the background scene—are introduced through Eqs. (3)-(5) for the current statistics.

The method described above, using Rice's equation to evaluate search set performance against uniform scenes, is well known [4,14]. Since a target's presence in the scene would necessarily render the scene non-uniform, and since the method based on Rice's equation is valid only for uniform scenes, Rice's equation can be used to calculate FAR, but not P_D.

The first method presented for calculating search set performance against non-uniform scenes is given in the Non-Uniform Scenes Subsection. Although this method is a simple, heuristic, extension of the well-known uniform background result reviewed in the subsection on Uniform Scenes, it appears to be original. The heuristic approach of the subsection on Non-Uniform Scenes has the advantage of being both easy to understand and easy to apply. Moreover, comparison with rigorous methods indicates that the heuristic method yields numerically accurate performance predictions as long as the variations in the background scene are not too rapid [17,18].

The IRST performance model developed in the Analysis Section is a rigorous generalization of the Rice equation method. In fact, a point-by-point correspondence can be established between the simple, well-known analysis of the Uniform Scenes Subsection and the more general, new analysis in this report.

Appendix A generalizes Eq. (3).

Appendix B generalizes Eqs. (4) and (5).

Eq. (55), originally derived by Cramér and Leadbetter [19], generalizes Eq. (9).

As expected, the analysis in this report reduces exactly to the simple Rice equation method in the uniform background limit. More generally, the method developed in this report is also applicable to non-uniform scenes (i.e., scenes containing targets and/or structured backgrounds).

The techniques developed in this report are applied to the evaluation of a number of candidate signal processing structures in a companion paper to the present work [18].

It is noted that tracking algorithms are neither modeled nor discussed, although they may play an important role in clutter rejection as well as target tracking [20]. Moreover, no consideration is given to the availability of target and backgound infrared radiance data suitable as model inputs. No strategies are proposed for synthesizing IRST processor structures to satisfy either *a priori* performance requirements or optimization criteria. The contribution of this paper is the formulation of a performance analysis model: Complete descriptions of an IRST sensor and the radiance distribution of a particular scene are required as inputs. As output, the model generates the probability that the IRST device declares (rightly or wrongly) a target's presence in the given scene.

SCANNING BLIP SENSORS: ELEMENTARY CONCEPTS

A Basic Threshold Receiver

In order to provide a frame of reference for the following discussion, it is necessary to describe a simple IRST receiver structure, and to define the parameters used to characterize IRST performance.

The probability that the IRST device makes a target declaration when a target is in fact in the sensor's field of view is called the Probability of Detection (P_D). The average rate at which false target declarations occur is termed the false-alarm rate (FAR).

A basic threshold comparison receiver is shown in Fig. 1. The current $X(t)$ at the output of the detector is input to an electrical filter of transfer function $H(f)$. The output current $Y(t)$ of the electrical filter is compared with a threshold $Y_0(t)$. If $Y(t)$ exceeds the threshold, the presence of a "target" is declared; otherwise, no target declaration is made. Target detections and false alarms are both manifested as threshold crossings, suggesting the following approach to IRST performance assessment:

- The expected number of threshold crossings that a particular processor experiences against a given infrared scene is first calculated. As discussed in Appendix C, the expected number of threshold crossings during a given time interval may be interpreted as a probability of target declaration.

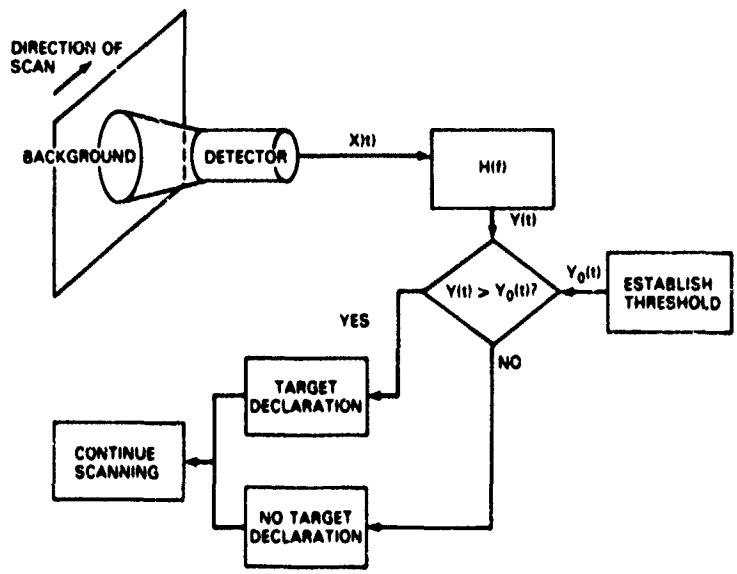

Fig 1 – A basic threshold comparison receiver. The photodetector in this figure is "idealized", in the sense that it is presumed to have a perfect all-pass electrical frequency characteristic; the frequency-dependent part of the detector responsivity is lumped together with the transfer function of the post-detector filter to obtain $H(f)$. A "target declaration" is made whenever the filtered current $Y(t)$ exceeds the threshold level $Y_0(t)$

- If the specified scene is known to contain a target, the computed probability of target declaration is interpreted as a Probability of Detection (P_D); otherwise, a False Alarm Rate (FAR) interpretation is given.

As will presently be discussed, it is highly desirable that the threshold-establishing mechanism suppress clutter-induced threshold crossings by increasing $Y_0(t)$ when $Y(t)$ is "clutter-like."

Rather than allow $Y_0(t)$ to take on an *a priori* constant or functional value, it is necessary to establish the threshold by some means that "adapts" $Y_0(t)$ to the prevailing background conditions.

A similar type of signal processing problem has been addressed in the radar [21,22] and sonar [23] literatures. A candidate adaptive threshold scheme adapted from the earlier work [24] is depicted in Fig. 2.

The block with transfer function $\exp(-j2\pi fT_d)$ introduces a delay of T_d seconds. The triangular-shaped block in this figure denotes an ideal all-pass amplifier of gain K. Note that the delay time T_d, gain K, and transfer functions $H_0(f)$ and $H(f)$ are all design variables. Strategies for choosing the design variables in order to satisfy particular performance requirements or optimization criteria will not be discussed. This report is devoted to developing a formulation for the expected number of threshold crossings for IRST receivers structured as in Fig. 2, under the assumption that the design variables have all been specified.

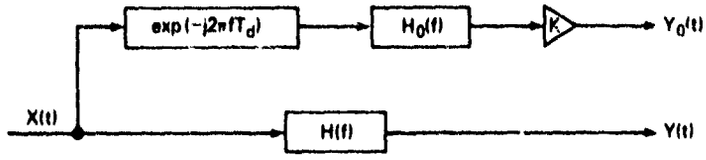

Fig. 2 — A simple adaptive threshold scheme is illustrated. The transfer function $\exp(-j2\pi f T_d)$ introduces a delay of T_d seconds, ensuring decorrelation of the random processes $Y(t)$ and $Y_0(t)$. The significance of the random currents is seen by inspection of Fig. 1.

Uniform Scenes

Current Statistics

When the sensor of Fig. 1 scans across a uniform background scene, the output current $Y(t)$ is "statistically stationary." The meaning of statistical stationarity will now be discussed as background to the discussion of non-uniform scenes and non-stationary processes that follow in the Non-Uniform Scenes subsection.

It is assumed that the sensor is scanned and re-scanned over the same scene, and that there are no changes in either the scene or the sensor from one scan to the next.

The current $y(t)$ during the course of any one particular scan is called a "sample function"* of the random process $Y(t)$. (The process $Y(t)$, in turn, may be thought of as the infinite ensemble of possible sample functions.) The current sample function obtained on the n^{th} scan is designated $y(t;n)$. We now consider a particular one of these sample functions, $y(t;1)$, depicted in Fig. 3.

The time variations in $y(t;1)$ have their origin in the time-of-arrival fluctuations of the individual photons incident on the detector.† Thus, the fluctuations in $y(t,1)$ are independent of the scan velocity and are present regardless of whether the sensor is scanning or motionless. The average current at a particular instant of time t_a may be defined as the "ensemble average":

$$m_1(t_a) \equiv \lim_{N\to\infty}\left\{\frac{1}{N}\sum_{n=1}^{N} y(t_a;n)\right\} \equiv E\{Y(t_a)\}. \tag{1}$$

In order for $Y(t)$ to be a stationary process, it is necessary that $m_1(t)$, as defined in Eq. (1), be independent of time. Thus,

$$m_1(t_a) = m_1(t_1),$$

*Consistent with a convention of random process theory, stochastic quantities are assigned capital letters, with sample values designated by the corresponding lower case letters.

†This kind of noise is often called "photon fluctuation noise" or "quantum noise." When the quantum noise associated with the background light is the dominant noise type in the sensor, the sensor is said to be operating in the "Background Limited Performance" (BLIP) regime.

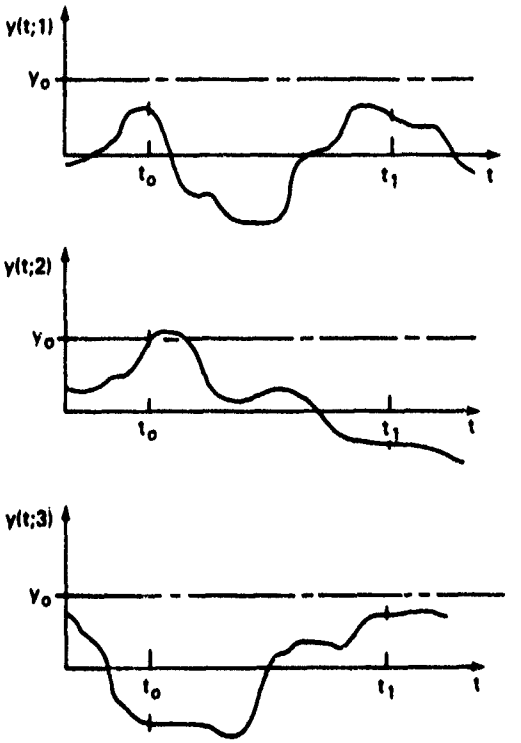

Fig. 3 — Three sample functions of the random current $Y(t)$ are shown as functions of time. The current $Y(t)$ is taken at the output of the post-detector filter as the sensor is scanned over a uniform scene (cf. Fig. 1). The sample functions are designated $y(t;n)$, $n = 1, 2, 3, \ldots$. The sample functions display random time variations caused by time-of-arrival fluctuations of the individual photons incident on the detector. Since the current $Y(t)$ is stationary, the ensemble average mean value (variance) defined by Eq. (1) (Eq. (2)) is the same at time t_0 as at time t_1, where times t_0 and t_1 are arbitrary.

where the times t_0 and t_1 are totally arbitrary (cf. Fig. 2). Similarly, the mean-square deviation of $Y(t)$ from its average value (i.e., the "variance" of Y) may be defined at each instant of time as

$$\sigma_Y^2(t) \equiv \lim_{N\to\infty}\left\{\frac{1}{N}\sum_{n=1}^{N}[Y(t;n) - m_Y(t)]^2\right\} \equiv E\{[Y(t)-m_Y(t)]^2\}. \tag{2}$$

The variance σ_Y^2, like the mean m_Y, is independent of time for stationary processes.

Equations (1) and (2) are satisfactory for illustrating the concept of "ensemble averaging"; however, it is desireable to have a different means for actually calculating the values of m_Y and σ_Y^2 in terms of standard background and sensor parameters.

It is first necessary to define the average value m_X of the current $X(t)$ (cf. Fig. 1):

$$m_X = E\{X(t)\} = \eta e m_Q, \tag{3}$$

where

η = quantum efficiency of the detector $\left[\frac{\text{electrons}}{\text{photon}}\right]$,

e = electronic charge $\left[\frac{\text{coulombs}}{\text{electron}}\right]$,

and

m_Q = average background photon flux $\left[\frac{\text{photons}}{\text{sec}}\right]$ incident on the detector.

It may be shown that for sensors operating in the BLIP regime the mean value and variance of $Y(t)$, originally defined by Eqs. (1) and (2), can be calculated in terms of m_X as follows:

$$m_Y = H(0)\, m_X, \tag{4}$$

and [25]

$$\sigma_Y^2 = 2em_X\Delta f, \tag{5}$$

where $H(0)$ is the zero-ordinate of the transfer function $H(f)$ (cf. Fig. 1), and Δf is the noise bandwidth of $H(f)$. For bandpass $H(f)$, $H(0) = 0$. It follows from Eq. (4) that $m_Y = 0$ for this case.

Since the scene is spatially uniform, the average photon flux m_Q is independent of time. It follows from Eqs. (3) - (5) that the mean m_Y and variance σ_Y^2 are also independent of time, justifying the claim of stationarity for the current $Y(t)$.

Assuming that the transfer function $H(f)$ is normalized as follows:

$$\max_f H(f) = 1, \tag{6}$$

the noise bandwidth Δf in Eq. (5) may be calculated from the equation:

$$\Delta f = \int_0^\infty |H(f)|^2\, df. \tag{7}$$

Crossing Rates for Fixed Threshold Detection

It is now assumed that the signal processor of Fig. 1 is implemented such that the threshold y_o is equal to a constant. The fixed threshold y_o is depicted on the sample function plots of Fig. 3. A brief outline will now be given of a method for calculating the average number of times m_J that the random process $Y(t)$ crosses the threshold during a time interval of duration T seconds. (The relationship between the mean number of crossings m_J and the usual search set performance parameters P_D and FAR is discussed in Appendix C.)

The expected number of threshold crossings $m_J(0,T)$ during the time interval $|t| < T/2$ may be written in terms of a "crossing rate" $\dot{m}_J$ as:

$$m_J(0,T) = \dot{m}_J T \tag{8}$$

According to Rice [16], $\dot{m}_J$ may be calculated as

$$\dot{m}_J = \dot{m}_{J_o} \exp(-u^2/2), \tag{9}$$

where

$$\dot{m}_{J_o} \equiv \left[\frac{1}{\Delta f}\int_0^\infty f^2 |H(f)|^2 df\right]^{1/2}, \tag{10}$$

with Δf given by Eq. (7). Also,

$$u \equiv (y_o - m_Y)/\sigma_Y, \tag{11}$$

with m_Y and σ_Y given by Eqs. (4) and (5).

The quantity u defined by Eq. (11) may be thought of as a normalized threshold level.

It follows from Eq. (9) that the expected number of threshold crossings drops off rapidly as the theshold level is increased

Finally, it should be noted that the uniform-background threshold crossing formalism described above cannot be used to calculate the expected number of threshold crossings associated with a target's presence in the scene*, because a target's presence would render the scene non-uniform.

Non-Uniform Scenes

Current Statistics

It is now assumed that the sensor of Fig. 1 is scanned a number of times over the same *non-uniform* scene, and that there are no changes in either the scene or the sensor from one scan to the next. A number of sample functions of the resulting current process $Y(t)$ are depicted in Fig. 4.

Once again, the ensemble average mean and variance of $Y(t)$ are defined by Eqs. (1) and (2). However, as discussed next, $Y(t)$ is now a non-stationary process, i.e., m_Y and σ_Y^2 are functions of time.

As an illustration of how such non-stationary processes arise, it is now assumed that the infrared scene encompasses regions of blue sky and clouds where

$m_Q(t_{BS})$ = average photon flux incident on the detector when blue sky is being observed,

and

$m_Q(t_C)$ = average photon flux incident on the detector when cloud is being observed.

The photon flux m_Q in Eq. (3) is seen to be a function of time: $m_Q(t)$ takes on the value $m_Q(t_C)$ at a time t_C when a cloud is in the field of view, and it takes on a different value $m_Q(t_{BS})$ at a time t_{BS} when the scanning field of view includes only blue sky. Thus, the process $Y(t)$ is non-stationary when the scene is non-uniform, because the mean and variance of $Y(t)$ are seen from Eqs. (3)-(5) to be functions of time†.

*As discussed in Appendix C, the incremental number of threshold crossings associated with a target's presence in the scene provides an estimate of the conventional search set parameter P_D. By definition, P_D is the probability of target detection

†For the present, it suffices to say that the forms of Eqs. (4) and (5) indicate that a time-varying m_X must give rise to time varying m_Y and σ_Y^2. However, it should be noted that Eqs. (4) and (5) are only strictly valid for stationary processes, i.e., for time-invariant m_X. Generalizations of Eqs. (4) and (5) valid for both stationary and non-stationary processes are given by Eqs. (B-30) and (B-31)

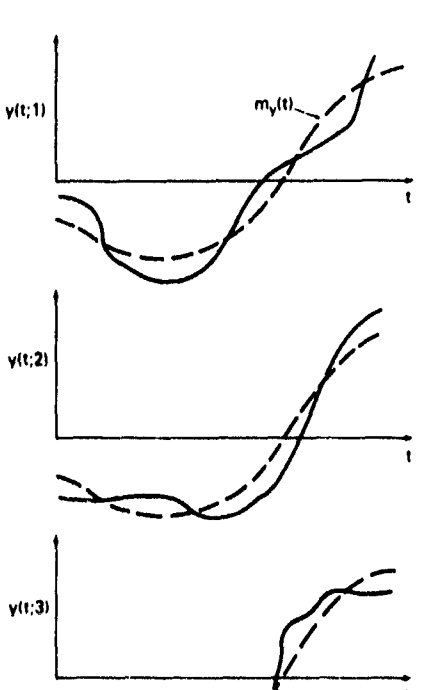

Fig. 4 — Three sample functions of the random current $Y(t)$ are shown as functions of time. This figure is similar to Fig. 3, except the sensor is now presumably scanned over a non-uniform scene. The time-varying ensemble average $m_Y(t)$ of $Y(t)$ is shown as a dashed curve superposed on each of the three depicted sample functions (solid curves). The ensemble average m_Y is still defined by Eq. (1); however, the fact that m_y is now a function of time implies that $Y(t)$ is now a nonstationary random process.

The time-varying mean value $m_Y(t)$ is superposed as a dashed curve on each of the sample functions $y(t)$ depicted in Fig. 4.

Crossing Rates for Fixed Threshold Detection

The performance of a fixed threshold signal processor (cf. Fig. 1) against a non-uniform scene can be characterized in terms of the quantity m_J, where*

$$m_J(0,T) \equiv E\{J\} = \int_{T_a} \dot{m}_J(t)\,dt, \tag{12}$$

where T_a is the time interval $|t| < T/2$, J is an integer random variable equal to the number of times that the current $Y(t)$ crosses the threshold level y_a during the time interval T_a, and $E\{.\}$ is the statistical expectation operator as defined in Eqs. (1) and (2). Equation (12) is a straightforward generalization of Eq. (8) to allow for the possibility of time-variable threshold crossing rates $\dot{m}_J$.

As long as the time variation of $m_Y(t)$ is slow compared to the time variation of the impulse response $h(t)$ of the post-detector filter (cf. Fig. 1), a good estimate for $\dot{m}_J(t)$ can be obtained from Eq. (9).

*Cf. Appendix C for a discussion of the relationship of $m_J(0, T)$ to the usual IRST performance parameters P_D and FAR.

The following steps are then followed in calculating $m_J(0,T)$:

a. The time-varying mean current $m_X(t)$ is derived from the time-varying photon irradiance $m_Q(t)$ by means of Eq. (3). (A detailed formulation for $m_X(t)$ in terms of the background radiance distribution is provided in Appendix A.)

b. Estimates of $m_Y(t)$ and $\sigma_Y^2(t)$ are obtained from Eqs. (4) and (5). (More rigorously, Eqs. (B-30) and (B-31) may be used to obtain $m_Y(t)$ and $\sigma_Y^2(t)$.)

c. Equation (11) is evaluated for the time-varying normalized threshold $u(t)$.

d. Equation (9) is evaluated for the time-varying threshold crossing rate $\dot{m}_J(t)$.

e. Equation (12) is evaluated for the expected number of threshold crossings $m_J(0, T)$.

Numerical examples following the above prescription typically show that the crossing rate function $\dot{m}_J(t)$ is extremely sharply peaked (cf. Fig. 5). Consequently, appreciable contributions to $m_J(0,T)$ only accrue in the near neighborhood of points such as t_p in Fig. 5. It is shown in Ref. 17 that the time t_p in Fig. 5b is a saddle point of the crossing rate integral Eq. (12), and that Eq. (12) may be approximated asymptotically as:

$$m_J(0, T) \simeq \dot{m}_J(t_p)\ \delta t_p, \tag{13}$$

with $\dot{m}_J(t_p)$ obtained from Eq. (9). The quantity δt_p is the effective interval of time during which $m_Y(t)$ remains in the near neighborhood of its peak value, from the standpoint of crossing rate calculations. An expression for δt_p is derived in Ref. 17.

The implications of Eq. (13) for system performance are illustrated with the aid of Fig. 6.

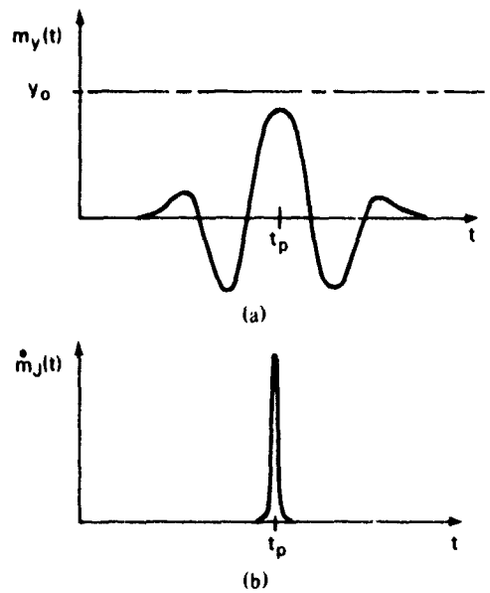

Fig. 5 — Part a) is an illustrative plot of $m_Y(t)$ vs t, where m_Y is the mean value of the filtered current $Y(t)$. Also shown is a constant threshold current Y_o, lying above the peak value of m_Y. The function $m_Y(t)$ takes on its peak value at the time t_p.

Part (b) is a plot of the threshold crossing rate $\dot{m}_J(t)$ corresponding to the threshold Y_o and mean current $m_Y(t)$ of part (a). The entire contribution to the crossing rate integral, Eq. (12), accrues in the very near neighborhood of t_p.

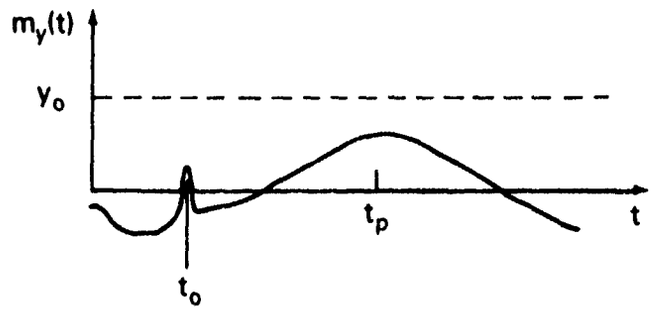

Fig. 6 — This figure illustrates a critical shortcoming of constant threshold processing. The slowly varying maximum centered at t_p presumably has its origin in the non-uniform background scene. The narrower, lower amplitude spike centered at t_o is due to a target. The likelihood of a false alarm (i.e., a clutter-induced threshold crossing) grows rapidly as the threshold level y_o is reduced. There is no way for the constant threshold processor to detect the target peak at t_o without also incurring a false alarm arising from the clutter peak centered at t_p.

A plot of the threshold crossing rate $\dot{m}_y(t)$ corresponding to this figure would show that the probability of a threshold crossing, and hence a false alarm, is far greater at time t_p than at any other time.

The large, relatively slowly varying maximum centered at t_p in Fig. 6 is presumed to have its origin in the background scene. The narrower, lower amplitude spike centered at t_o in Fig. 6 is presumed to be due to a "target."

It follows from Eqs. (13) and (9) that the likelihood of a clutter-induced threshold crossing grows rapidly as the threshold level y_o in Fig. 6 is lowered. A clutter-induced threshold crossing (i.e., a "false alarm") becomes a virtual certainty[6] when there is a "mean-crossing," *i.e.*, when the threshold level actually intercepts the mean current $m_y(t)$. [17,18] There is apparently no way for the constant threshold processor to detect the target peak at t_o without also incurring a false alarm arising from the clutter peak centered at t_p.

Crossing Rates for Constant False Alarm Rate (CFAR) Adaptive Threshold Detection

The performance of an adaptive-threshold processor is illustrated with the aid of Fig. 7.

The processor is presumed to have some means for deriving high-confidence estimates for $m_y(t)$ and $\sigma_y(t)$, defined as $\hat{m}_y$ and $\hat{\sigma}_y$, respectively. When $m_y(t)$ is "slowly-varying" the processor establishes $y_o(t)$ as:

$$y_o(t) = \hat{m}_y(t) + K\hat{\sigma}_y(t). \tag{14}$$

[6] This has been established by integrating the crossing rate function $\dot{m}_y$ over an interval of time containing a time point t_{mc} for which $m_y(t_{mc}) = y_o$. An asymptotic analysis (cf. Ref. 17) has shown that the crossing rate integral Eq. (12) is incremented by unity for each such time t_{mc} contained in the interval of integration T_o. This result is not at all surprising, and may be taken as evidence that the theory developed here is consistent with common sense.

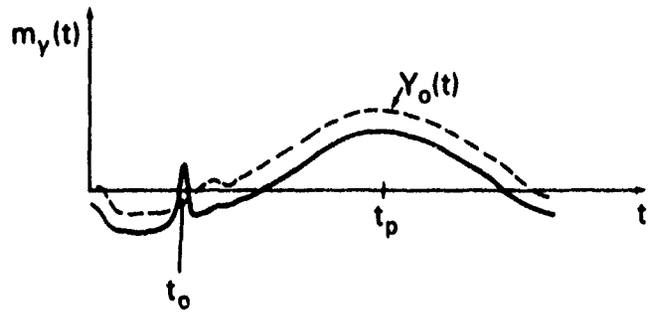

Fig. 7 — This figure illustrates an important potential advantage of adaptive threshold processing. The mean current $m_Y(t)$ is the same as for Fig. 6, with a clutter peak centered at time t_p, and a lower-amplitude target spike centered at time t_o. The adaptive threshold $v_o(t)$ is presumably able to accurately track the slowly varying background signal, but not the more rapidly varying target signal. Thus, target detection is assured, while the probability of a false alarm is kept acceptably small. As contrasted with the situation of Fig. 6, the probability of a false alarm is now no greater in the neighborhood of time t_p than at any other time.

The threshold is interpolated through periods of "rapidly varying" $m_1(t)$ by means of a smoothing filter (cf., for example, the neighborhood of t_o in Fig. 7). The adaptive-threshold constant K in Eq. (14) is a design parameter.

From Eqs. (11) and (14),

$$u(t) = K[\hat{\sigma}_1(t)/\sigma_1(t)] + \left[\hat{m}_1(t) - m_1(t)\right]/\sigma_1(t). \tag{15}$$

When the estimation errors are sufficiently small,

$$\hat{\sigma}_1(t) \simeq \sigma_1(t), \tag{16}$$

and

$$\hat{m}_1(t) \simeq m_1(t),$$

it follows from Eq. (15) that

$$u(t) \simeq K. \tag{17}$$

Thus, $u(t)$ is rendered time-invariant by the adaptive-threshold processor when there is no rapidly-varying target contribution to $m_1(t)$. When there are no targets in the scene, the mean current $m_1(t)$ is assumed to be slowly-varying, and the expected number of crossings during the time interval T_o may be calculated from Eqs. (9), (12), and (17) as

$$m_J(0, T) = \int_{T_o} \dot{m}_{J_o} \exp(-K^2/2)\, dt. \tag{18}$$

Since both $\dot{m}_{J_o}$ and K are time-invariant, Eq. (18) becomes

$$m_J(0, T) = \dot{m}_{J_o} \exp(-K^2/2)\, T. \tag{19}$$

Equation (19) has the same form as the crossing rate expression for uniform scenes, Eq. (8).

The kind of processor just described has been called a constant false alarm rate (CFAR) processor, since the threshold crossing rate is now independent of time, i.e., a crossing is no more likely to occur when scanning a region of non-uniform background than when scanning a region of uniform background. For example, with reference to Fig. 7, the crossing rate is now no greater at t_p than at any other time.

Unfortunately, the CFAR processor is generally a non-realizable ideal: it has been assumed that the processor is able to estimate the quantities $m_Y(t)$ and $\sigma_Y(t)$ to as high a precision as desired. Errors in the estimated values for m_Y and σ_Y are usually unavoidable, giving rise to appreciable time-dependence in Eq. (15) for $u(t)$.

ANALYSIS

Introduction

The objective of the next subsection is to present an expression for the expected value of the number of times a nonstationary noise $Y(t)$ crosses a nonstationary stochastic threshold $Y_o(t)$.

The crossing-rate formulation that results, Eqs. (25) and (27), requires knowledge of the joint density function $f_{YY\dot{Y}_o\dot{Y}_o}$ of the current $Y(t)$, its time derivative $\dot{Y}(t)$, the threshold $Y_o(t)$, and its time derivative $\dot{Y}_o(t)$.

As discussed in Ref. 17, the currents $Y(t)$ and $Y_o(t)$ are non-stationary Gaussian processes. It follows that $Y(t)$, $\dot{Y}(t)$, $Y_o(t)$, and $\dot{Y}_o(t)$, are jointly Gaussian processes. The joint density $f_{YY\dot{Y}_o\dot{Y}_o}$ can thus be expressed in terms of a covariance matrix Λ.

Assuming that the filtered current $Y(t)$ and the threshold $Y_o(t)$ are uncorrelated processes, the fourth-order density function factorizes into

$$f_{YY\dot{Y}_o\dot{Y}_o} = f_{YY}\, f_{\dot{Y}_o\dot{Y}_o}. \tag{20}$$

The justification for Eq. (20) is discussed in the next section. Expression (52) for the jointly Gaussian $f_{Y\dot{Y}}$ is then used with the general crossing rate Expression (48) to derive a more explicit crossing rate expression, Eq. (55). Evaluation of Eq. (55) for $\dot{m}_J$ requires the expressions derived in Appendix B for the time-varying current statistics $\sigma_Z(t)$, $\sigma_Y(t)$, and $r(t)$ (cf. Eqs. (B-30) - (B-34)).

The complete expression for the average crossing rate, Eq. (47), generally requires the numerical integration of a somewhat complicated integrand. The section called Crossing Rates for Adaptive Threshold Processors is devoted to deriving an approximation to Eq. (47). The result, Eq. (67), is the principal analytical result of this report.

A Basic Equation for Curve Crossing Rates

The integer random variable J is defined as the number of zero-crossings of a random process $G(t)$ on a time interval $|t| < T/2$. The expected value of J is defined as $m_J(0, T)$. Thus,

$$m_J(0, T) = E\{J\}, \tag{21}$$

where $E\{.\}$ denotes an ensemble average. Defining the crossing rate function $\dot{m}_J(t)$ as in Eq. (12), it can be shown that (cf. Ref. 26, p. 514)

$$\dot{m}_J(t) = \int |\dot{g}| f_{GG}(0,\dot{g})\, d\dot{g}. \tag{22}$$

The function $f_{G\dot{G}}$ in Eq. (22) is the joint probability density function of the process $G(t)$ and its time derivative $\dot{G}(t)$.

Equation (22) is well known; however, most references to it appear to impose a stationarity requirement on G that is not actually necessary. The applicability of this equation to nonstationary processes appears to have first been recognized by Cramér and Leadbetter [19].

The domain of integration in Eq. (22) is a matter of some interest. If one wishes to calculate only the expected number of positive slope zero-crossings, i.e., the expected number of times that both

$$G(t_o) = 0 \tag{23}$$

and

$$\dot{G}(t_o) > 0 \tag{24}$$

are both satisfied on the interval $|t| < T/2$, the lower and upper limits of integration in Eq. (22) should be chosen as 0 and ∞, respectively. The resulting expression for $m_J(0, T)$,

$$m_J(0,T) = \int_{T_o} dt \left\{ \int_o^\infty d\dot{g}\ |\dot{g}| f_{G\dot{G}}(0,\dot{g}) \right\}, \tag{25}$$

does not include zero-crossings of the type depicted in Fig. 8, for which $\dot{g} < 0$. Apparently, $\dot{m}_J$ is sensitive only to the "right type" of zero crossing, as defined by the limits of integration in Eq. (22).

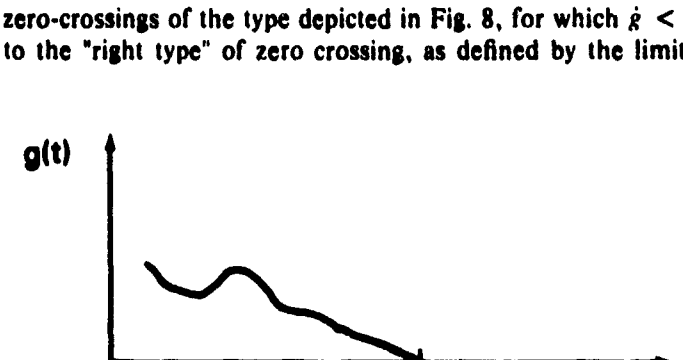

Fig 8 — A sample function $g(t)$ of the random process $G(t)$ is depicted as a function of time. The particular sample function chosen has a down-crossing at time t_o

The process $G(t)$ is now assumed to be formed as the difference of two stochastic processes $Y(t)$ and $Y_o(t)$. Thus,

$$G(t) \equiv Y(t) - Y_o(t), \tag{26}$$

where $Y_o(t)$ is referred to as the "threshold process". Without making any assumptions with respect to the statistics of $Y(t)$ and $Y_o(t)$ (e.g., each process may be both nonstationary and non-Gaussian) it follows from Eq. (26) that

$$f_{G\dot{G}}(0,\dot{g}) = \int\int d\zeta d\eta \, f_{Y\dot{Y}Y_o\dot{Y}_o}(\zeta,\dot{g}+\eta,\zeta,\eta). \tag{27}$$

The proof of this equation is straight-forward (cf. Ref. 27, p. 131). Assuming that the processes, $Y, \dot{Y}, Y_o$, and $\dot{Y}_o$, are jointly Gaussian (cf. Ref. 17 for justification), their joint density can be expressed in terms of their covariance matrix [27] Λ. The matrix Λ has four rows and four columns, for a total of sixteen elements. Written in partitioned form, we have

$$\Lambda = \begin{Vmatrix} \mathbf{C} & \mathbf{C}_1^T \\ \mathbf{C}_1 & \mathbf{C}_o \end{Vmatrix}, \tag{28}$$

where the superscript T denotes the matrix transpose operation. The submatrices $\mathbf{C}$, $\mathbf{C}_o$, and $\mathbf{C}_1$ are defined as

$$\mathbf{C} = \begin{Vmatrix} \sigma_Y^2(t) & C_{Y\dot{Y}}(t,t) \\ C_{\dot{Y}Y}(t,t) & \sigma_{\dot{Y}}^2(t) \end{Vmatrix}, \tag{29}$$

$$\mathbf{C}_o = \begin{Vmatrix} \sigma_{Y_o}^2(t) & C_{Y_o\dot{Y}_o}(t,t) \\ C_{Y_oY_o}(t,t) & \sigma_{\dot{Y}_o}^2(t) \end{Vmatrix}, \tag{30}$$

and

$$\mathbf{C}_1 = \begin{Vmatrix} C_{Y_oY}(t,t) & C_{Y_o\dot{Y}}(t,t) \\ C_{\dot{Y}_oY}(t,t) & C_{\dot{Y}_o\dot{Y}}(t,t) \end{Vmatrix}. \tag{31}$$

The scalar covariances that comprise these elements are defined by

$$C_{AB}(t_1,t_2) \equiv E\Big\{\big[A(t_1) - m_A(t_1)\big]\big[B(t_2) - m_B(t_2)\big]\Big\}, \tag{32}$$

where A and B take on the values Y, $\dot{Y}$, Y_o, and $\dot{Y}_o$, as appropriate. Also,

$$m_A(t) \equiv E[A(t)] \tag{33}$$

and

$$\sigma_A^2(t) \equiv C_{AA}(t,t). \tag{34}$$

It follows from Eq. (32) that $C_{Y\dot{Y}}(t,t) = C_{\dot{Y}Y}(t,t)$ and $C_{Y_oY_o}(t,t) = C_{Y_oY_o}(t,t)$. Thus, the matrices $\mathbf{C}$ and $\mathbf{C}_o$ are symmetric.

The elements of C are obtained directly from Eqs. (B-17), (B-20), and (B-23):

$$\sigma_Y^2(t) = e\{m_X(t) \circledcirc h^2(t)\}, \tag{35}$$

$$\sigma_{\dot{Y}}^2(t,t) = e\{m_X(t) \circledcirc [\dot{h}(t)]^2\}, \tag{36}$$

and

$$C_{Y\dot{Y}}(t,t) = \sigma_Y(t)\,\dot{\sigma}_Y(t), \tag{37}$$

where e is the electronic charge, $h(t)$ is the impulse response of the post-detector filter (cf. Fig. 1), $m_X(t)$ is the mean value of the current $X(t)$ (cf. Fig. 1), and $\circledcirc$ is the convolution operator:

$$f(t) \circledcirc g(t) \equiv \int_{-\infty}^{\infty} f(t-x)g(x)\,dx. \tag{37a}$$

The relationship of $m_X(t)$ to the radiance of the scene under observation and the optical parameters of the IRST sensor is discussed in Appendix A, and expressed quantitatively by Eq. (A-2).

Expressions for the elements of Eq. (30) may be obtained as direct adaptations of Eqs. (35) (37). It follows from Fig. 2 that

$$Y_o(t) = Kh_o(t-T_d) \circledcirc X(t), \tag{38}$$

where $h_o(t)$ is the Fourier inverse of $H_o(f)$. Taking the expected value of both sides of this equation, we have

$$m_{Y_o}(t) = Kh_o(t-T_d) \circledcirc m_X(t), \tag{39}$$

which is analagous to Eq. (B-30). It may also be shown, analagous to Eqs. (35) - (37) that:

$$\sigma_{Y_o}^2(t) = eKm_X(t) \circledcirc h_o^2(t-T_d), \tag{40}$$

$$\sigma_{\dot{Y}_o}^2(t) = eKm_X(t) \circledcirc [\dot{h}_o(t-T_d)]^2, \tag{41}$$

and

$$C_{Y_oY_o}(t,t) = \sigma_{Y_o}(t)\,\dot{\sigma}_{Y_o}(t). \tag{42}$$

It remains only to formulate similar expressions for the elements of C_1 in order to complete the specification of the joint density $f_{Y\dot{Y}Y_o\dot{Y}_o}$.

Assuming that the processes $Y(t)$ and $Y_o(t)$ are both derived from the process $X(t)$ by means of the structure shown in Fig. 2, it is shown in Ref. 17 that, if

$$h_o(t-T_d)\,h(t) = 0, \tag{43}$$

then

$$\mathbf{C}_1 = 0. \tag{44}$$

That is, choosing a sufficiently long time delay T_d in Fig. 2 validates the factorization of the fourth order density $f_{YY_oY_o}$ into the product of two second order densities:

$$f_{YY_oY_o}(y,\dot{y},y_o,\dot{y}_o) = f_{Y\dot{Y}}(y,\dot{y})\,f_{Y_oY_o}(y_o,\dot{y}_o). \tag{45}$$

From Eqs. (22), (27), and (45),

$$\dot{m}_J(t) = \int\int d\zeta d\eta\, f_{Y_o\dot{Y}_o}(\zeta,\eta)\left\{\int d\dot{g}\,|\dot{g}|\,f_{\dot{Y}\ddot{Y}}(\zeta,\dot{g}+\eta)\right\}. \tag{46}$$

With the change of variable $z = \dot{g}+\eta$, Eq. (46) may be written

$$\dot{m}_J(t) = E_{Y_o\dot{Y}_o}\left\{\dot{m}_J(t|y_o,\dot{y}_o)\right\}, \tag{47}$$

where, by definition,

$$\dot{m}_J(t|y_o,\dot{y}_o) \equiv \int_{\dot{Y}_o}^{\infty} |z-\dot{y}_o|\,f_{\dot{Y}\ddot{Y}}(y_o,z)\,dz, \tag{48}$$

and

$$E_{Y_o\dot{Y}_o}[.] \equiv \int\int d\zeta d\eta\, f_{Y_o\dot{Y}_o}(\zeta,\eta)\,[.] \tag{49}$$

The quantity $\dot{m}_J$, previously interpreted as the zero-crossing rate of the process G (cf. Eq. (22)), is now interpreted as the threshold crossing rate of the process $Y(t)$ (cf. Eq. (47)).

The quantity

$$\dot{m}_J(t|y_o,\dot{y}_o) \equiv \dot{m}_J(t|\cdot) \tag{50}$$

defined by Eq. (48) will be referred to as the "threshold-conditional crossing rate."

Non-Stationary Gaussian Processes

Further development of Eq. (48) for the threshold-conditional crossing rate is contingent on obtaining a suitable expression for the joint density $f_{Y\dot{Y}}$. The objective of this section is to evaluate Eq. (48) for the particular case of a bivariate Gaussian density, Eq. (52).

The justification for assuming a Gaussian distribution for f_Y (and hence for $f_{\dot{Y}}$ and $f_{\ddot{Y}}$ as well) is discussed in Ref. 17. As shown in Ref. 17, the relative error in $\dot{m}_J$ is approximately equal to the relative error ϵ in the density function of $Y(t)$.

$$f_Y(y) \simeq \sigma_Y^{-1}\,\phi\left(\frac{y-m_Y}{\sigma_Y}\right)(1+\epsilon), \tag{51}$$

where $\phi(.)$ is the Gaussian density function, Eq. (57). The Edgeworth series expansion [16] of $f_Y(y)$ provides a simple and easily evaluated expression for the relative error ϵ. Sample calculations described in Ref. [17] show that ϵ is negligibly small for typical system and background parameter values. Thus, the joint density $f_{Y\dot{Y}}$ is now assumed to have the following bivariate normal form:

$$f_{Y\dot{Y}}(y_o,z) = \left\{2\pi\sigma_Y\sigma_{\dot{Y}}(1-r^2)^{1/2}\right\}^{-1}\exp\left\{-\left[\frac{u^2+v^2-2ruv}{2(1-r^2)}\right]\right\}, \tag{52}$$

where the quantities m_Y, σ_Y, $\sigma_{\dot{Y}}$, and r, are obtained from Eqs. (B-30) - (B-34). Also,

$$u \equiv (y_o - m_Y)/\sigma_Y \tag{53}$$

and

$$v \equiv (z - m_Z)/\sigma_Z. \tag{54}$$

Substituting Eq. (52) into Eq. (48), it may be shown that [17]

$$\dot{m}_J(t|y_o,\dot{y}_o) = \left(\frac{\sigma_Z}{\sigma_Y}\right)(1-r^2)^{1/2}\,\phi(u)\,\{\phi(p) + p\,\Phi(p)\}, \tag{55}$$

where, by definition:

$$p \equiv \left[(1-r^2)^{1/2}\,\sigma_Z\right]^{-1}(m_Z + ru\sigma_Z - \dot{y}_o). \tag{56}$$

The functions $\phi(.)$ and $\Phi(.)$ in Eq. (55) are defined as follows:

$$\phi(x) \equiv (2\pi)^{-1/2}\exp(-x^2/2) \tag{57}$$

and

$$\Phi(x) \equiv \int_{-\infty}^{x} \phi(z)\,dz \tag{58}$$

The crossing rate Eq. (55) is originally due to Cramér and Leadbetter [19].

Equations (47) and (55), together, represent a formal means for calculating the mean threshold crossing performance of the adaptive threshold processor depicted in Fig. 2. However, the evaluation of Eq. (47) appears to present some significant calculational difficulties. These difficulties are obviated by means of the approximate method of evaluation pursued in the following section.

Crossing Rates for Adaptive Threshold Processors

Numerical results obtained thus far indicate that the correlation coefficients r and r_o are typically much less than unity, as follows:

$$|r(t)| = |C_{YY}(t,t)\,[\sigma_Y(t)\sigma_Y(t)]^{-1}| << 1 \tag{59}$$

and

$$|r_o(t)| = |C_{Y_o Y_o}(t,t)\,[\sigma_{Y_o}(t)\,\sigma_{Y_o}(t)]^{-1}| << 1, \tag{60}$$

where Eq. (59) comes from Eq. (B-24), and Eq. (60) is obtained by analogy to Eq. (59).

It follows from Eqs. (47) and (49) that the threshold crossing rate for stochastic threshold functions $Y_o(t)$ may be written as

$$m_J(t) = \int_{-\infty}^{\infty}\int d\zeta\,d\eta\;\dot{m}_J(t|\zeta,\eta)\,f_{Y_o Y_o}(\zeta,\eta). \tag{61}$$

Equations (59) and (60) permit considerable simplification of the functions appearing inside the integral in Eq. (61).

From Eqs. (55) and (59):

$$\dot{m}_J(t|\zeta,\eta) \cong \left|\frac{\sigma_Z}{\sigma_Y}\right| \phi(u)\{\phi(p) + p\Phi(p)\}, \tag{62}$$

where u, $\phi(\cdot)$, and $\Phi(\cdot)$, are given by Eqs. (53), (57), and (58), respectively. From Eqs. (56) and (59),

$$p \cong (m_Z - \eta)/\sigma_Z. \tag{63}$$

By analogy with Eq. (52), and making use of Eq. (60),

$$f_{Y_a Y_a}(\zeta,\eta) = \left\{\sigma_{Y_a}^{-1}\, \phi(u_a)\right\}\left\{\sigma_{Z_a}^{-1}\, \phi(p_a)\right\}, \tag{64}$$

where u_a and p_a are defined similarly to Eqs. (53) and (63) as

$$u_a \equiv (\zeta - m_{Y_a})/\sigma_{Y_a} \tag{65}$$

and

$$p_a \equiv (m_{Z_a} - \zeta)/\sigma_{Z_a}. \tag{66}$$

It follows from Eqs. (61) - (66) and some algebra that

$$\dot{m}_J(t) = (2\pi)^{-1/2}\left|\frac{\sigma_{ZZ_a}}{\sigma_{YY_a}}\right| \phi\left|\frac{m_{Y_a} - m_Y}{\sigma_{YY_a}}\right| F(m_{Z_a} - m_Z), \tag{67}$$

where, by definition

$$\sigma^2_{Y_a} \equiv \sigma^2_Y + \sigma^2_a \tag{68}$$

and

$$\sigma^2_{ZZ_a} \equiv \sigma^2_Z + \sigma^2_a. \tag{69}$$

The quantities $m_{Y_a}(t)$, $\sigma_{Y_a}(t)$, and $\sigma_{YY_a}(t)$, in Eqs. (67) - (69) are calculated by means of Eqs. (39), (40), and (41), respectively. Finally, the expected number of threshold crossings in a time interval T_a may be obtained as

$$m_J(0,T) = \int_{T_a} \dot{m}_J(t)\, dt, \tag{70}$$

with $\dot{m}_J(t)$ given by Eq. (67).

Equation (67) provides the basis for analyzing a much broader range of possible adaptive threshold schemes than Fig. 2 might suggest. For example, straightforward generalizations of Eq. (67) may be applied to the structures depicted in Figs. 9-11.

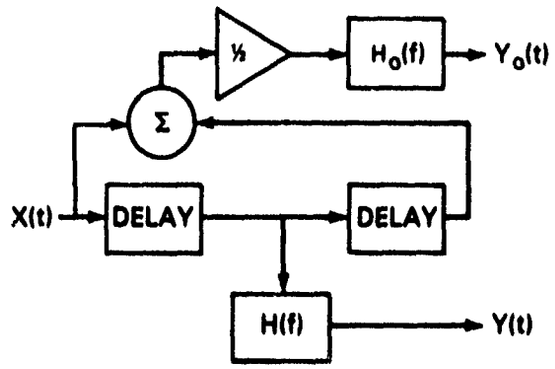

Fig. 9 — An adaptive threshold scheme is illustrated. Each of the delay elements introduces a delay of T_d seconds. The significance of the random currents $Y(t)$, $Y(t)$, and $Y_0(t)$ is seen by inspection of Fig. 1. The block diagram shown here is actually just one part of the threshold processing receiver shown in Fig. 1.

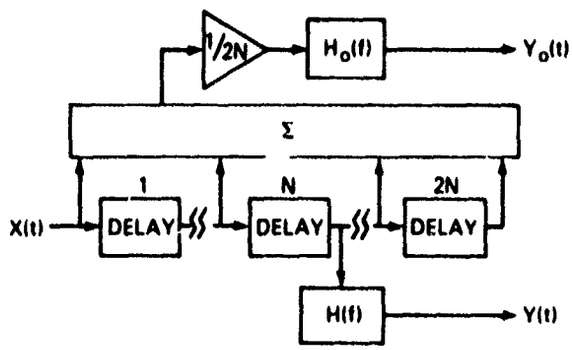

Fig. 10 — A candidate adaptive threshold scheme is illustrated that generalizes the structure of Fig. 9. The threshold-establishing approach shown here is realized in terms of a tapped delay line with 2N taps. Once again, the significance of $Y(t)$, $Y(t)$, and $Y_0(t)$, follows from Fig. 1.

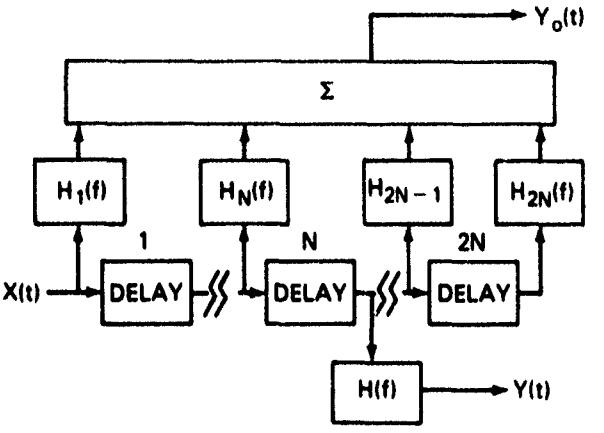

Fig. 11 — The tapped delay line adaptive threshold scheme shown here generalizes the structure of Fig. 10. The transfer functions $H_n(f)$, $n = 1, 2, \ldots, 2N$ at each of the $2N$ taps of the tapped delay line are design variables, chosen to maximize the receiver's performance against a particular background scene, or set of background scenes. There is no *a priori* reason why the various delays should be chosen as equal to one another, other than for fabricational simplicity. More generally, additional degrees of freedom are incorporated by allowing these delays to take on distinct values.

While the function $F(m_{\ell_n} - m_\ell)$ in Eq. (67) is fairly complicated, its zero-ordinate is unity:

$$F(0) = 1. \tag{71}$$

Equation (71) is a highly desireable feature, as explained in the next section.

It is noted that for uniform backgrounds,*

$$(\sigma_{\ell_n}/\sigma_\ell)^2 = (\Delta f_n/\Delta f) \tag{72}$$

and

$$(\sigma_{\ell_n}/\sigma_\ell)^2 \cong (\Delta f_n/\Delta f)^3, \tag{73}$$

where Δf is the noise bandwidth of $H(f)$, and Δf_n is the noise bandwidth of $H_n(f)$ (cf. Fig. 2). It follows from Eqs. (68), (69), (72), and (73) that

$$\sigma^2_{\ell_n} = \sigma^2_\ell \left\{1 + (\Delta f_n/\Delta f)\right\} \tag{74}$$

and

$$\sigma^2_{\ell_n} \cong \sigma^2_\ell \left\{1 + (\Delta f_n/\Delta f)^3\right\}. \tag{75}$$

*Eq. (73) is derived by assuming a rectangular-shaped $H(f)$ having an upper cut-off frequency f_n and a noise bandwidth $\Delta f \simeq f_n$

Equations (74) and (75) are good approximations so long as $m_Y(t)$ is slowly varying compared to $h(t)$ and $h_n(t)$.

DISCUSSION

Experience with the numerical evaluation of Eq. (70), with $\dot{m}_J(t)$ given by Eq. (67), has shown that the principal contributions to the integral m_J of $\dot{m}_J$ accrue in the neighborhood of a discrete set of times.

Moreover, it has been shown that these important discrete times are of two types: "mean-crossing times," and "times of closest approach" [17].

Mean-crossing times t_{mc} satisfy the following two conditions simultaneously:

$$m_Y(t_{mc}) = m_{Y_n}(t_{mc}) \tag{76}$$

and

$$\dot{m}_Y(t_{mc}) > \dot{m}_{Y_n}(t_{mc}). \tag{77}$$

For each solution of Eq. (76) that satisfies constraint (77), i.e., each time the mean current $m_Y(t)$ crosses the mean threshold $m_{Y_n}(t)$ with positive slope, the expected number of crossings m_J is incremented by unity. Whenever mean-crossings exist during the interval T_n, it is generally not necessary to perform the integral of Eq. (70); in this case, the expected number of threshold crossings $m_J(O,T)$ is well-approximated by the number of mean-crossing times t_{mc} during the interval T_n. Clearly, it is desireable that no mean-crossing times exist except when there is a target in the scene, this may be taken as a reasonable first principle of search set design for operation against structured backgrounds.

If $m_Y(t)$ lies below $m_{Y_n}(t)$ on the time interval T_n, i.e., if there are no mean-crossings during T_n, the crossing count integral Eq. (70) is generally dominated by contributions accruing in the neighborhood of "closest approach times" t_{ca}, where by definition

$$m_J(t_{ca}) = m_{J_n}(t_{ca}) \tag{78}$$

It follows from Eqs. (67), (71), and (78), that the mean threshold crossing rate for adaptive-threshold (AT) processors is

$$\dot{m}_{JI}(t) = (2\pi)^{-1/2} \left[\frac{\sigma_{J/n}}{\sigma_Y}\right] \phi\left[\frac{m_{Y_n} - m_Y}{\sigma_{Y_n}}\right] \tag{79}$$

in the neighborhood of all closest approach times. Thus, the complicated function $I(\cdot)$ appearing in Eq. (67) is generally not needed in evaluating Eq. (70).

Analogous to Eq. (79), the mean threshold crossing rate for fixed-threshold (FT) processors is given by

$$\dot{m}_{JI}(t) = \dot{m}_J(t|y_n, 0) = (2\pi)^{-1/2} \left[\frac{\sigma_J}{\sigma_Y}\right] \phi\left[\frac{y_n - m_Y}{\sigma_Y}\right]. \tag{80}$$

Equation (80) is derived from the background-conditional crossing rate, Eq. (62), by imposing a saddle point condition analagous to Eq. (78):

$$p = (m_Z - \dot{y}_0)/\sigma_{\dot{Y}} = 0. \tag{81}$$

Alternatively, Eq. (80) may be derived by noting that for fixed threshold processors:

$$\sigma^2_{\dot{Y}_0} = \sigma^2_{Y_0} \equiv 0 \tag{82}$$

and

$$m_{Y_0} \equiv y_0. \tag{83}$$

From Eqs. (68), (69), and (82),

$$\sigma^2_{\dot{Y}Y_0} \equiv \sigma^2_{\dot{Y}} \tag{84}$$

and

$$\sigma^2_{\dot{Y}Z_0} \equiv \sigma^2_{\dot{Y}} \tag{85}$$

for fixed-threshold processors. Substituting Eqs. (83) - (85) into Eq. (79), the adaptive-threshold crossing rate $\dot{m}_{1T}$ is seen to reduce properly to the fixed-threshold crossing rate $\dot{m}_{1T}$ given by Eq. (80).

The advantages and disadvantages of adaptive threshold (AT) processing vis-á-vis fixed threshold (FT) processing may be evaluated by comparing the crossing-rate expressions in Eqs. (79) and (80).

It follows from Eq. (80) that fixed threshold processors will suffer background-induced mean-crossings whenever the peak target amplitude is less than the clutter amplitude. This situation is depicted in Fig. 6. Thus, it may be said that target-to-clutter ratios less then unity cause the FT processor performance to be "background-structure-limited" (BSL). In this case, each "false alarm" can be associated with a structural feature in the backgound. The effect of quantum noise (as reflected in the magnitude of $\sigma_{\dot{Y}}$, for example) is then totally overshadowed by background structure effects.

Inspection of Eq. (79) and Fig. 7 shows that an Adaptive Threshold (AT) processor need not suffer background-induced mean-crossings. If the filter $H_0(f)$ (cf. Fig. 2) can be chosen such that $m_{\dot{Y}_0}(t)$ "tracks" the background-induced variations in $m_{\dot{Y}}(t)$, the background-induced mean-crossings can be eliminated.

Such false alarms as then occur are distributed randomly in time, and are not associated with particular features in the background scene: the residual false alarms are due to quantum noise. An IRST sensor operating in this regime (e.g., Fig. 7) is said to be "quantum-noise-limited" (QNL) in its performance. Clearly, QNL (quantum-noise-limited) operation is preferable to BSL (background-structure-limited) operation.

It should be noted that the adaptive threshold performance advantage just described is only realized when the background scene is non-uniform. The performance of AT processors is generally inferior to the performance of FT processors when the background scene is uniform

and of known brightness. In this case, the adaptive threshold false alarm rate (FAR_{AT}) is greater (i.e., worse) than the fixed threshold false-alarm rate (FAR_{FT}):

$$FAR_{AT} > FAR_{FT}. \tag{86}$$

In order to make the false alarm rate comparison above meaningful, it is assumed that the adaptive-threshold gain K in Fig. 2 has been adjusted to achieve equal target-detection sensitivities for the two processors being compared.*

A false-alarm penalty (FAP) is now defined:

$$FAP \equiv 10\log_{10}(FAR_{AT}/FAR_{FT}). \tag{87}$$

The false-alarm penalty is a measure of the performance disadvantage that accrues when an AT processor is used when it truly isn't needed. Eq. (87) may be written as

$$FAP = 10\log_{10}(\dot{m}_{AT}/\dot{m}_{FT}) \quad \text{dB}. \tag{88}$$

with $\dot{m}_{AT}$ and $\dot{m}_{FT}$ given by Eqs. (79) and (80), respectively. The evaluation of Eq. (88) is simplified considerably by making use of Eqs. (74) and (75). It follows from Eqs. (74), (75), (79), (80), and (88) that:

$$FAP = 2.17\left(\frac{\alpha}{1+\alpha}\right)\left(\frac{m_{Y_a}-m_Y}{\sigma_Y}\right)^2 + 5\log_{10}[1-\alpha(1-\alpha)], \text{ dB}, \tag{89}$$

where, by definition,

$$\alpha \equiv \left(\frac{\Delta f_a}{\Delta f}\right). \tag{90}$$

Equation (89) simplifies still further in the limit $\alpha << 1$. Thus

$$FAP = 2.17\,\alpha\left[\left(\frac{m_{Y_a}-m_Y}{\sigma_Y}\right)^2 - 1\right] \quad \text{dB}, \alpha << 1. \tag{91}$$

As an example, it is assumed that the threshold-constant K in Fig. 2 is adjusted until " the threshold is five sigmas above the mean," i.e.,

$$\left(\frac{m_{Y_a}-m_Y}{\sigma_Y}\right) = 5 \tag{92}$$

when the search set is observing a uniform scene of known brightness. Furthermore, it is assumed that the noise bandwidth of the target filter $H(f)$ in Fig. 2 is twice as large as the noise bandwidth of the threshold-setting-filter $H_a(f)$,

$$\alpha = \left(\frac{\Delta f_a}{\Delta f}\right) = \frac{1}{2}. \tag{93}$$

*It is assumed that the threshold filter $H_a(f)$ responds too slowly to suppress fast rise-time target-induced threshold crossings

It follows from Eqs. (89), (92), and (93) that the false alarm penalty is:

$$FAP = 17.46 \text{ dB}, \tag{94}$$

corresponding to a value of FAR_{AT} (adaptive threshold false-alarm rate) about 56 times worse than FAR_{FT} (fixed-threshold false-alarm rate).

Generally, Δf_n should be chosen smaller than Δf to both minimize the false alarm penalty, (Eq. (89)), and to prevent a too-rapid threshold response that would tend to suppress target-induced threshold crossings. On the other hand, Δf_n should be chosen large enough to allow the threshold to accurately follow most of the structure in the background scene. Clearly, the choice for Δf_n involves degrading system performance against uniform backgrounds for the sake of improved performance against non-uniform backgrounds.

It appears likely that a more favorable trade-off could be achieved with the receiver structure shown in Fig. 9, both from the standpoint of (a) decreasing the false alarm penalty, Eq. (89), and (b) improving the background tracking properties of $m_{Y_n}(t)$. Equation (79) and the entire analysis of the preceding section is easily adapted to the structures of Figs. 9-11. The false-alarm penalty, Eq. (89), decreases roughly as $(2N)^{-1/2}$ for the detector of Fig. 10. The improvement in uniform background performance thus obtained for large values of N is gained at the expense of degraded performance against cluttered scenes, as compared to detectors with small values of N. The good background-tracking capability of the structure in Fig. 9 combined with the low false-alarm penalty of the structure of Fig. 10 can be obtained by employing a two-dimensional-detector array with time-delay and integration (TDI) logic.

In order to put this discussion on a concrete quantitative basis, particular background and target radiance distributions must be chosen, and the mean current $m_1(t)$ calculated by means of Eq. (A-2) in Appendix A. The target detection and clutter rejection capabilities of a given candidate adaptive-threshold processor can then be analyzed by means of Eq. (79). Intercomparisons of the numerical results thus obtained for a variety of different processor structures should then allow quantitative conclusions to be drawn concerning such issues as:

- The performance penalty caused by failing to match the sensor's instantaneous field-of-view to the angular size of the target.

- The potential performance advantages of time-delay and integration (TDI).

- The best value of N, and the desireability of having different transfer functions $H_n(f)$ for each of the $2N$ taps in the tapped delay line structure of Fig. 11.

- The advantages that may be gained by employing two-dimensional threshold processing, in which the "target signal" $Y(t)$ and threshold function $Y_n(t)$ are derived from detectors scanning at different elevations.

The only important obstacle to performing analyses of the kind described above is the lack of high-spatial-resolution, radiometric, infrared background imagery.

Appendix A

CALCULATING THE AVERAGE PHOTOCURRENT FROM BACKGROUND DATA

The objective of this Appendix is to present Eq. (A-2), which expresses the average value of the random current $X(t)$ (cf. Fig. 1),

$$m_X(t) = E[X(t)], \tag{A-1}$$

as a function of the scene radiance distribution $m_L(\mathbf{r})$ and a number of important sensor parameters.

As derived in Ref. 17,

$$m_X(t) = K_n R_I \int \mathrm{MTF}(\mathbf{f})\, \mathcal{P}(\mathbf{f})\, m_{\mathcal{S}}(\mathbf{f}) \exp(j2\pi \mathbf{f}\cdot\mathbf{v}t)\, d\mathbf{f}. \tag{A-2}$$

The various quantities appearing on the right-hand-side of Eq. (A-2) will now be defined.

The constant K_n is given by

$$K_n = \pi \tau_n / (2f^{\#})^2, \tag{A-3}$$

where τ_n is the transmittance of the optics, and $f^{\#}$ is the focal length ratio of the optics.

The constant R_I is the current responsivity, given by:

$$R_I = \eta e / h\nu, \tag{A-4}$$

where η is the detector quantum efficiency, e is the electronic charge, h is Planck's constant, and ν is the average optical frequency of the incident light.

The variable of integration in Eq. (A-2), $\mathbf{f}$, is the two-dimensional vector spatial frequency. The quantity $\mathrm{MTF}(\mathbf{f})$ is the modulation transfer function that characterizes the image blurring effect of the optical train, normalized such that

$$\mathrm{MTF}(\mathbf{0}) = 1. \tag{A-5}$$

For the detector geometry depicted in Fig. A1, the quantity $P(\mathbf{r})$ is defined as follows:

$$P(\mathbf{r}) = \begin{cases} 1 & \mathbf{r} \in \mathcal{A}_{det} \\ 0 & \mathbf{r} \in \mathcal{A}_{det}^{c} \end{cases} \tag{A-6}$$

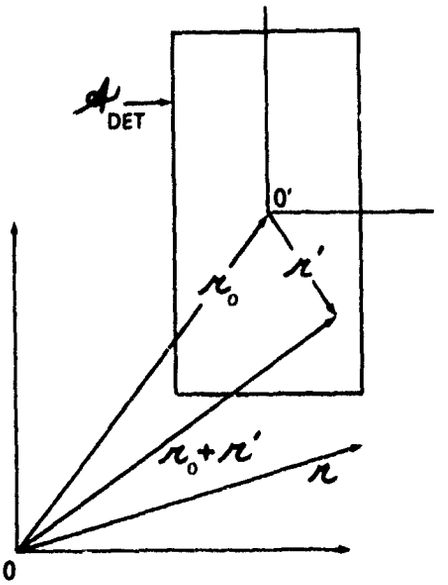

Fig A1 — Focal Plane Geometry. The focal plane irradiance is stationary in the coordinate system with origin 0. Vector r_o locates the center of a detector of area A_{det}. For scanning sensors, r_o is a function of time

The function $\mathcal{P}(\mathbf{f})$ is defined as the two-dimensional spatial Fourier transform of $P(\mathbf{r})$:

$$\mathcal{P}(\mathbf{f}) = \int P(\mathbf{r}) \exp(j2\pi \mathbf{f}\cdot\mathbf{r}) d\mathbf{r}, \tag{A-7}$$

Similarly, $m_f(\mathbf{f})$ is the two-dimensional spatial Fourier transform of the radiance distribution $m_l(\mathbf{r})$. It should be noted that $m_l(\mathbf{r})$, like $m_l(t)$ in Eq. (A-2), is an ensemble average value over the photon fluctuation statistics of the incident light.

The radiance distribution $m_l(\mathbf{r})$ is characteristic of a particular infrared scene, and may be estimated by means of a radiometric Thermal Imaging System [1,2] (TIS) of higher spatial resolution than the model system. It is also highly desirable that the dwell time of the TIS be much longer than that of the model system, since the analysis requires knowledge of the mean radiance of the scene established by averaging over the photon fluctuation statistics of the incident light*.

The spectral filter chosen for use with the TIS should match the combined TIS optical train/photodetector spectral response to that of the model system. This is necessary because there is no way to reliably calculate the radiance of a scene measured in a waveband $\Delta\lambda_1$ in terms of the radiance of the same scene measured in a different spectral band $\Delta\lambda_2$.

The quantity v in Eq. (A-2) is the focal plane scan velocity, which may be calculated as

$$|\mathbf{v}| = 2\pi f^{\#} D_{ap}/T_f, \tag{A-8}$$

where D_{ap} is the diameter of the optical aperture, and T_f is the system frame time.

*Averaging out the photon noise by either increasing the TIS dwell time or by performing frame addition decreases the noisiness of the TIS image, and improves the goodness of the TIS imagery as an estimate of $m_l(\mathbf{r})$

Appendix B
NOISE CURRENT CORRELATION FUNCTIONS

The object of this Appendix is to derive Eqs. (B-30) - (B-34), which are needed to evaluate Eq. (55) for the threshold crossing rate $\dot{m}_J(t|y_n, \dot{y}_n)$.

The starting point for this discussion is the linear system input/output relation between the random processes $X(t)$ and $Y(t)$ (cf. Figure 1):

$$Y(t) = \int_{-\infty}^{\infty} d\mu \; X(\mu) h(t-\mu). \tag{B-1}$$

It follows directly from Eq. (B-1) that

$$C_{YY}(t_1, t_2) = \int\int_{-\infty}^{\infty} d\mu d\lambda \; C_{XX}(\lambda, \mu) \; h(t_1-\lambda) \; h(t_2-\mu), \tag{B-2}$$

where the covariances C_{YY} and C_{XX} are defined by

$$C_{YY}(t_1, t_2) \equiv E\{[Y(t_1) - m_Y(t_1)] \; [Y(t_2)-m_Y(t_2)]\}, \tag{B-3}$$

$$C_{XX}(\lambda, \mu) \equiv E\{[X(\lambda)-m_X(\lambda)] \; [X(\mu)-m_X(\mu)]\}, \tag{B-4}$$

and where

$$m_Y(t) \equiv E\{Y(t)\}, \tag{B-5}$$

and

$$m_X(t) \equiv E\{X(t)\}. \tag{B-6}$$

With the definition

$$Z(t) \equiv \dot{Y}(t), \tag{B-7}$$

it follows from Eq. (B-3) that

$$C_{YZ}(t_1, t_2) = \partial_{t_2} \{C_{YY}(t_1, t_2)\} \tag{B-8}$$

and

$$C_{ZZ}(t_1, t_2) = \partial_{t_1} \partial_{t_2} \{C_{YY}(t_1, t_2)\}. \tag{B-9}$$

From Eqs. (B-2), (B-8), and (B-9),

$$C_{YZ}(t_1, t_2) = \int\int_{-\infty}^{\infty} d\mu d\lambda \; C_{XX}(\lambda, \mu) \; h(t_1-\lambda) \; \partial_{t_2} h(t_2-\mu) \tag{B-10}$$

and

$$C_{ZZ}(t_1, t_2) = \int\int_{-\infty}^{\infty} d\mu d\lambda \; C_{XX}(\lambda, \mu) \; \partial_{t_1} h(t_1-\lambda) \; \partial_{t_2} h(t_2-\mu). \tag{B-11}$$

Setting $t_1 = t_2 = t$ in Eqs. (B-10) and (B-11), and noting that

$$C_{ZZ}(t, t) = \sigma_Z^2(t) = E\{Z^2(t)\} - m_Z^2(t), \tag{B-12}$$

it follows that

$$C_{YZ}(t, t) = \int\int_{-\infty}^{\infty} d\mu d\lambda \; C_{XX}(\lambda, \mu)\, h(t-\lambda)\, \partial_t h(t-\lambda) \tag{B-13}$$

and

$$\sigma_Z^2(t) = \int\int_{-\infty}^{\infty} d\mu d\lambda \; C_{XX}(\lambda, \mu)\, \partial_t h(t-\lambda)\, \partial_t h(t-\mu). \tag{B-14}$$

Setting $t_1 = t_2 = t$ in Eq. (B-2), and noting that

$$C_{YY}(t,t) = \sigma_Y^2(t) = E\{Y^2(t)\} - m_Y^2(t), \tag{B-15}$$

it follows that

$$\sigma_Y^2(t) = \int\int_{-\infty}^{\infty} d\mu d\lambda \; C_{XX}(\lambda, \mu) h(t-\lambda) h(t-\mu). \tag{B-16}$$

An expression for $C_{XX}(\lambda, \mu)$ is now required before the analysis can be carried any further. An adaptation of Eq. (4.3.13) on p. 115 of Ref. 28 leads to:

$$\sigma_Y^2(t) = e \int_{-\infty}^{\infty} d\mu \; h^2(t-\mu)\; m_X(\mu), \tag{B-17}$$

where e is the electronic charge. Consistency between Eqs. (B-16) and (B-17) requires that

$$C_{XX}(\lambda, \mu) = e\, m_X(\mu)\, \delta(\lambda - \mu), \tag{B-18}$$

where $\delta(.)$ is the Dirac delta function. Covariance functions like Eq. (B-18) are characteristic of non-stationary white noise [26,29]. From Eqs. (B-13), (B-14), and (B-18),

$$C_{YZ}(t, t) = e \int_{-\infty}^{\infty} d\mu \; h(t-\mu)\, \partial_t h(t-\mu)\, m_X(\mu) \tag{B-19}$$

and

$$\sigma_Z^2(t) = e \int_{-\infty}^{\infty} d\mu \; [\partial_t h(t-\mu)]^2\, m_X(\mu). \tag{B-20}$$

Noting that

$$h(t-\mu)\, \partial_t h(t-\mu) = \frac{1}{2}\, \partial_t h^2(t-\mu), \tag{B-21}$$

it follows from Eqs. (B-19) and (B-21) that

$$C_{YZ}(t, t) = \frac{1}{2}\, e \partial_t \left\{ \int_{-\infty}^{\infty} d\mu \; h^2(t-\mu)\; m_X(\mu) \right\}. \tag{B-22}$$

From Eqs. (B-17) and (B-22),

$$C_{YZ}(t, t) = \frac{1}{2}\, \partial_t \{\sigma_Y^2(t)\} = \sigma_Y(t)\, \dot{\sigma}_Y(t). \tag{B-23}$$

Defining $r(t)$ as

$$r(t) = C_{YZ}(t, t)\, [\sigma_Y(t) \sigma_Z(t)]^{-1}, \tag{B-24}$$

it follows from (B-23) and (B-24) that

$$r(t) = \{\dot{\sigma}_Y(t)/\sigma_Z(t)\}. \tag{B-25}$$

Taking the expected value of both sides of Eq. (B-1) leads to the result:

$$m_Y(t) = \int_{-\infty}^{\infty} d\mu \; m_X(\mu)\; h(t-\mu). \tag{B-26}$$

Taking the time derivative of (B-1), we have

$$\dot{Y}(t) = Z(t) = \int_{-\infty}^{\infty} d\mu \; X(\mu)\; \partial_t h(t-\mu). \tag{B-27}$$

Taking the expected value of both sides of (B-27), we have

$$m_Z(t) = \int_{-\infty}^{\infty} d\mu \; m_X(\mu)\; \partial_t h(t-\mu).$$

That is,

$$m_Z(t) = \partial_t \left\{ \int_{-\infty}^{\infty} d\mu \; m_Y(\mu)\; h(t-\mu) \right\}. \tag{B-28}$$

From Eqs. (B-26) and (B-28),

$$m_Z(t) = \dot{m}_Y(t). \tag{B-29}$$

Defining the convolution operator as in Eq. (37a), Eqs. (B-26), (B-17), (B-20), (B-29), and (B-25) may be written as:

$$m_Y(t) = h(t) \circledast m_X(t), \tag{B-30}$$

$$\sigma_Y^2(t) = e\; h^2(t) \circledast m_1(t), \tag{B-31}$$

$$\sigma_Z^2(t) = e[\dot{h}(t)]^2 \circledast m_Y(t), \tag{B-32}$$

$$m_Z(t) = \dot{m}_1(t), \tag{B-33}$$

and

$$r(t) = \{\dot{\sigma}_1(t)/\sigma_Z(t)\}. \tag{B-34}$$

Equations (B-30) - (B-34) are the desired results.

Appendix C
RELATIONSHIPS BETWEEN FAR, P_D, and m_J

Relationship Between FAR and m_J

The complete description of an IRST sensor's performance under a given set of operational conditions requires the simultaneous specification of both the False Alarm Rate (FAR) and the Probability of Detection (P_D) for a "target" within the sensor's field of view. However, both "false alarms" and target detections are manifested as threshold crossings by the signal processor. Thus, the object of this Appendix is to relate the traditional IRST performance measures, P_D and FAR, to the expected number of threshold crossings m_J over prescribed intervals of time.

It is assumed that the average current $m_Y(t)$ is known* on an interval of time $|t| < T/2$.

The expected number of threshold crossings on the interval $|t| < T/2$ is defined as $m_J(0, T)$. Defining the false alarm rate as the expected number of threshold crossings per "reference interval" T_{ref}, the following relationship obtains between FAR and m_J:

$$\text{FAR} = (T_{ref}/T)\, m_J(0, T). \qquad \text{(C-1)}$$

For example, if FAR is defined as the average number of false alarms per week, T_{ref} is set equal to the number of seconds in one week; if FAR is defined as the average number of false alarms per system dwell time, then T_{ref} is set equal to the dwell time (again expressed in units of seconds).

It is implicitly assumed in Eq. (C-1) that the scene under observation does not include a target, so that each threshold crossing that occurs gives rise to a "false alarm."

Relationship Between P_D and m_J: First-Order Approximation

Although not as straight-forward as Eq. (C-1), a relationship between P_D and m_J can also be established.

As prelude to the definition of P_D, a "decision interval" T_D is first defined. The interval T_D is presumed to bracket the entire period of time during which the current $Y(t)$ manifests target-induced fluctuations.

Assuming that a target is present in the scene, the number of threshold crossings that occur during the interval T_D is defined as the integer random variable J. The discrete probability density function of J is denoted as $f_J(t)$.

*The quantity $m_Y(t)$ may be specified *a priori*, or it may be calculated in terms of the radiance of a particular background scene (as discussed in Appendix A).

The probability of detection P_D is now defined as the probability that one or more threshold crossings occur during the decision interval:

$$P_D = \sum_{j=1}^{\infty} f_J(j) \tag{C-2}$$

(The likelihood of a background-induced crossing during T_D has been neglected.) Unfortunately, the problem of obtaining a formulation for f_J appears to be quite difficult [30]. The focus of this paper has been on the development of formulations for the expected number of threshold crossings:

$$m_J \equiv E[J] = \sum_{j=1}^{\infty} j f_J(j). \tag{C-3}$$

In order to establish a relationship between P_D and m_J, Eqs. (C-2) and (C-3) are written as:

$$P_D = f_J(1) + \sum_{j=2}^{\infty} f_J(j) \tag{C-4}$$

and

$$m_J = f_J(1) + \sum_{j=2}^{\infty} j f_J(j). \tag{C-5}$$

Assuming that the probability of two or more threshold crossings is negligible during the decision interval T_D, Eqs. (C-4) and (C-5) can be estimated as

$$P_D \simeq f_J(1) \tag{C-6}$$

and

$$m_J \simeq f_J(1). \tag{C-7}$$

It follows from (C-6) and (C-7) that

$$P_D \simeq m_J(0, T_d). \tag{C-8}$$

According to Eq. (C-8), the expected number of threshold crossings during the decision interval T_D provides a good estimate of the detection probability P_D, so long as the probability of two or more crossings during T_D is negligible.

Relationship Between P_D and m_J: Proposal for a Second-Order Approximation

It appears only reasonable that an improved estimate could be obtained for P_D if the variance σ_J^2 of J were known in addition to the mean m_J of J. It will now be shown how knowledge of σ_J^2 can be used to calculate a second-order approximation for P_D (compare with Eqs. (C-4) and (C-6)):

$$P_D \simeq f_J(1) + f_J(2). \tag{C-9}$$

Unfortunately, the technique described in this section for calculating the second-order approximation to P_D cannot be implemented until a formulation for σ_J^2 is developed analagous

to Eq. (67) for $\dot{m}_J$. In this connection, it is noted that Bendat has derived an equation for the crossing count variance of stationary processes [31] His result (cf. also Ref. 30) is far more complicated than the analagous Eqs. (8) and (9) for m_J. Thus, a generalization of Bendat's result for σ_J^2 to the case of nonstationary processes and stochastic threshold functions may prove to be a difficult problem. Nonetheless, it is now assumed that a formulation for σ_J^2 can be obtained, analagous to the development for m_J as noted above and found in the main text. Analagous to Eq. (C-3),

$$\sigma_J^2 \equiv \left\{ \sum_{j=1}^{\infty} j^2 f_J(j) \right\} - m_J^2. \tag{C-10}$$

Substituting Eq. (C-3) into Eq. (C-10) leads to the following expression for σ_J^2:

$$\sigma_J^2 = f_J(1) \left[1 - f_J(1) \right] + 4 f_J(2) \left[1 - f_J(1) - f_J(2) \right] + E_J, \tag{C-11}$$

where

$$E_J \equiv \sum_{j=3}^{\infty} j^2 f - 2 \left[f(1) + 2f(2) \right] \sum_{j=3}^{\infty} jf - \left[\sum_{j=3}^{\infty} jf \right]^2. \tag{C-12}$$

Assuming that the probability of three or more threshold crossings is negligible during the decision interval, Eqs. (C-3) and (C-11) are approximated as:

$$m_J \simeq f_J(1) + 2f_J(2) \tag{C-13}$$

and

$$\sigma_J^2 \simeq f_J(1) \left[1 - f_J(1) \right] + 4 f_J(2) \left[1 - f_J(1) - f_J(2) \right]. \tag{C-14}$$

Calculation of m_J from Eqs. (67) and (70), and an analagous calculation for σ_J^2, enables Eqs. (C-13) and (C-14) to be solved for approximations to $f_J(1)$ and $f_J(2)$. The second-order approximation to P_D is then obtained by means of Eq. (C-9).

If Eq. (C-9) is found to yield an appreciably different result than Eq. (C-6), third-order or even higher-order approximations to P_D may be required; otherwise, the first-order Eq. (C-6) is then verified as a good approximation for P_D.

REFERENCES

1. J. M. Lloyd, *Thermal Imaging Systems*, Plenum Press, New York (1975).

2. "The Fundamentals of Thermal Imaging Systems" (F. Rosell and G. Harvey, editors) EOTPO Report No. 46, Naval Research Laboratory, Washington, D.C.

3. *Handbook of Military Infrared Technology*, (W. L. Wolfe, editor) U.S. Gov't. Printing Office, Washington, D.C. (1965).

4. K. Seyrafi, "Electro-Optical Systems Analysis," Electro-Optical Research Company, Los Angeles (1973).

5. L. M. Biberman, *Reticles in Electro-Optical Devices*, Pergamon Press, London, England (1966).

6. J. A. Jamieson, et al., *Infrared Physics and Engineering*, McGraw-Hill, New York (1963).

7. H. Samuelsson, "Infrared Systems: I. Expressions for Signal and Background Induced Noise with Space Filters," *IEEE Transactions on Aerospace and Electronic Systems* AES-7:27, Jan. 1971.

8. H. Samuelsson, "Infrared Systems: II. Accuracy of Angle Measurement", *IEEE Transactions on Aerospace and Electronic Systems* AES-7:34, Jan. 1971.

9. R. C. Jones, "New Method of Describing and Measuring the Granularity of Photographic Materials," *J. Opt. Soc. Am.* 45:799, Oct. 1955.

10. J. B. Thomas, *An Introduction to Statistical Communication Theory*, John Wiley and Sons, New York (1969).

11. W. B. Davnport, Jr. and W. L. Root, *An Introduction to the Theory of Random Signals and Noise*, McGraw-Hill, New York, (1958).

12. D. Z. Robinson, "Methods of Background Description and Their Utility", *Proceedings of the IRE* 47:1554 (1959).

13. L. M. Biberman, "Background Considerations in Infrared System Design", *Applied Optics*, 4: 343, March 1965.

14. *Electro-Optics Handbook*, RCA, Burlington, Mass. (1968).

15. R.H. Genoud, "Infrared Search-System Range Performance," *Proc. Inst. Radio Engrs.* 47:1581 (1959).

16. S. O. Rice, *Mathematical Analysis of Random Noise*, Selected Papers on Noise and Stochastic Processes (edited by N. Wax) Dover Publications, New York (1954).

17. R.A. Steinberg, "Passive Infrared Surveillance with Background-Limited Sensors: New Methods of Analysis," NRL Memorandum Report, Naval Research Laboratory, Washington, D.C. (to be published as an NRL Report).

18. R.A. Steinberg, "Passive Infrared Surveillance, Part II: Threshold Crossing Receivers." (to be published as an NRL Report).

19. H. Cramér and M.R. Leadbetter, *Stationary and Related Stochastic Processes.* John Wiley & Sons, New York, (1967).

20. G.V Trunk, "Survey of Radar Signal Processing," NRL Report 8117, Naval Research Laboratory, Washington, D.C., June 21,1977.

21a. R. Nitzberg, "Constant-False-Alarm-Rate Signal Processors for Several Types of Interference", *IEEE Transactions on Aerospace and Electronic Systems* **AES-8**:27, Jan. 1972.

21b. R. Nitzberg, "Constant-False-Alarm-Rate Processors for Locally Nonstationary Clutter," *IEEE Transactions on Aerospace and Electronic Systems* **AES-9**: 399, May 1973.

21c. R. Nitzberg, "Analysis of the Arithmetic Mean CFAR Normalizer for Fluctuating Targets," *IEEE Transactions on Aerospace and Electronic Systems* **AES-14**: 44, Jan. 1978.

22. J. T. Rickard, G. M. Dillard, "Adaptive Detection Algorithms for Multiple-Target Situations," *IEEE Transactions on Aerospace and Electronic Systems* **AES-13**: 338, July 1977.

23. D. V. Gupta, J.F. Vetelino, T.J. Curry and J.T. Francis, "An Adaptive Threshold System for Nonstationary Noise Backgrounds," *IEEE Transactions on Aerospace and Electronic Systems* **AES-13**: 11 Jan. 1977.

24. D.J. Torrieri, "Adaptive Thresholding Systems," *IEEE Transactions on Aerospace and Electronic Systems*, **AES-13**:273, May 1977.

25. W. K. Pratt, *Laser Communications Systems*, John Wiley and Sons, New York (1969).

26. A. Papoulis, *Probability, Random Variables, and Stochastic Processes*, McGraw-Hill, New York (1965).

27. J. L. Melsa and A. P. Sage, *An Introduction to Probability and Stochastic Processes*, Prentice-Hall, Inc., Englewood Cliffs, N.J. (1973).

28. R. M. Gagliardi and S. Karp, *Optical Communications*, John Wiley & Sons, New York (1976).

29. A. Papoulis, "Identification of Systems Driven by Nonstationary Noise," *IEEE Transactions on Information Theory* **IT-24**:240, March 1978.

30. I. F. Blake and W. C. Lindsey, "Level-Crossing Problems for Random Processes," *IEEE Transactions on Information Theory* **IT-19**:295, May 1973.

31. J.S. Bendat, *Principles and Applications of Random Noise Theory*, John Wiley and Sons, New York, (1958).